ACS APPLIED MATERIALS & INTERFACES

Research Article

www.acsami.org

Optimization of Chemical Structure of Schottky-Type Selection Diode for Crossbar Resistive Memory

Gun Hwan Kim,[†] Jong Ho Lee,[†] Woojin Jeon,[†] Seul Ji Song,[†] Jun Yeong Seok,[†] Jung Ho Yoon,[†] Kyung Jean Yoon,[†] Tae Joo Park,[‡] and Cheol Seong Hwang*,[†]

[†]WCU Hybrid Materials Program, Department of Materials Science and Engineering and Inter-university Semiconductor Research Center, Seoul National University, Seoul 151-744, Korea

[‡]Department of Materials Engineering, Hanyang University, Ansan, 426-791, Korea

ABSTRACT: The electrical performances of Pt/TiO_2/Ti/Pt stacked Schottky-type diode (SD) was systematically examined, and this performance is dependent on the chemical structures of the each layer and their interfaces. The Ti layers containing a tolerable amount of oxygen showed metallic electrical conduction characteristics, which was confirmed by sheet resistance measurement with elevating the temperature, transmission line measurement (TLM), and Auger electron spectroscopy (AES) analysis. However, the chemical structure of SD stack and resulting electrical properties were crucially affected by the dissolved oxygen concentration in the Ti layers. The lower oxidation potential of the Ti layer with initially higher oxygen concentration suppressed the oxygen deficiency of the overlying TiO_2 layer induced by consumption of the oxygen from TiO_2 layer. This structure results in the lower reverse current of SDs without significant degradation of forward-state current. Conductive atomic force microscopy (CAFM) analysis showed the current conduction through the local conduction paths in the presented SDs, which guarantees a sufficient forward-current density as a selection device for highly integrated crossbar array resistive memory.

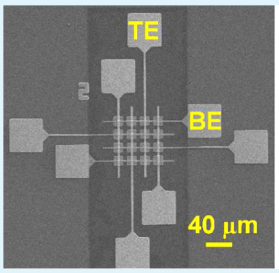

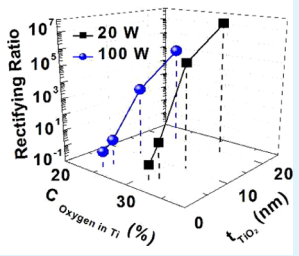

KEYWORDS: *Schottky diode, RRAM, crossbar, sneak current, selection device, Schottky barrier*

INTRODUCTION

Intensive research works have been performed to make breakthroughs with respect to the size and scale limit of the electronic devices. Among the various candidates for next-generation non-volatile memory, resistive switching random access memory (ReRAM) based on resistive switching (RS) phenomenon has been considered as a leading contender, because of its fast switching, excellent retention, and scalability.[1−3] In addition, its application to crossbar array (CA) is expected to offer great potential, because of its smaller cell area ($4F^2$, where F is the minimum feature size), easy fabrication process, three-dimensional (3D) stackability, and various application fields.[3−5] However, the realization of CA is still impeded by several obstacles. Among them, the most serious obstacle is undesirable leakage currents (sneak current) through the on-state unselected memory cells, which hinders the electric signal from selected cell. To solve the sneak current problem, various selection devices, such as the $p-n$ junction-type diode,[5,6] Schottky-type diode (SD),[7−9] threshold switching (TS) device,[10,11] complementary resistive switching (CRS) device,[12] and self-rectifying RS device,[13] have been intensively studied.

Among the various selection devices, SDs show superior performance, with high rectifying ratio and high forward-current density through a localized current path,[7,14] which is essential for largely integrated CA devices. Although the unidirectional rectifying characteristic of SDs is not suitable enough to use it for bipolar resistive switching devices, its promising selection performance for CA is remarkable, compared to other selection devices. In addition, SDs are advantageous to the situation of serial connection with RS memory cell, because SD is independent from the operation voltages of memory (unlike TS- or CRS-type devices), which would cause serious operational failure due to voltage division during dynamic resistance change of devices. Despite the many advantages that SD has, the performance of SD is seriously dependent on the chemical structures of its stacked layers, which govern the electrical conduction characteristics throughout the device. Since the required electrical specification of SDs depends on the integration density of CA, the guidance for the optimized chemical structures and fabrication processes for SDs is essential. Recently, the authors reported the highly promising performance of CA-type SDs with a rectification ratio of ~10^6 and a forward-current density of ~10^5 A cm^{-2}.[14] Such promising performances were achieved from the optimized structure of the Pt/TiO_2/Ti SD structure, where the Pt/TiO_2 and TiO_2/Ti interfaces constitute the Schottky and quasi-Ohmic junctions, respectively. Since the materials are of a polycrystalline nature, and their physical and chemical structure could have been changed largely according to the fabrication

Received: July 11, 2012
Accepted: September 21, 2012
Published: September 21, 2012

   dx.doi.org/10.1021/am301293v | *ACS Appl. Mater. Interfaces* 2012, 4, 5338−5345

conditions, the performance could be profoundly influenced by the fabrication steps. TiO_2 is especially vulnerable to oxygen vacancy formation, bceause of its relatively low bonding energy, which is actually beneficial to achieve the Ohmic-like contact with metal but is detrimental to the rectifying property of the Schottky junction, and Ti is a very reactive metal toward the reaction with oxygen during the deposition or oxygen ions in the TiO_2, which is in contact with itself in the SD structure. Therefore, the studies on the influences of the chemical structure of each layer in the SDs stack on the diode performance are impending but have been rarely reported.

In this work, the effects of chemical structure of Pt/TiO_2/Ti/Pt stacked capacitor-like SD devices on electrical performance were systematically examined. The chemical, physical, and electrical properties of the Ti layer were studied using Auger electron spectroscopy (AES) analysis, X-ray diffraction (XRD), transmission line measurement (TLM), and sheet resistance measurement by elevating the temperature. The chemical structures of TiO_2/Ti/Pt stacks were analyzed by AES and X-ray photoelectron spectroscopy (XPS) analysis, and their influence on the electrical performance of the SD were examined. It was revealed that the oxygen concentration of Ti layer and oxygen vacancies of TiO_2 layer crucially affect the rectifying characteristics of SDs. Conductive atomic force microscopy (CAFM) measurement was also performed to examine the variation of electrical conduction paths in forward- and reverse-biased states of SDs.

EXPERIMENTAL SECTION

Ti layers ~150 nm thick were grown on a Pt substrate [Pt(100 nm)/Ti(10 nm)/SiO_2(100 nm)/Si] via a dc magnetron sputtering method, using pure (99.999%) Ti metal targets in an Ar atmosphere under ambient conditions with a working pressure of ~6 mTorr at room temperature. The base pressure of the sputtering chamber was ~3×10^{-7} Torr. A dc power of 20 or 100 W was applied to the Ti target. The reason for choosing sputtering powers of 20 and 100 W was to achieve a significant difference in growth rate during Ti thin film deposition. Actually, detailed growth conditions can be varied, depending on the deposition systems, so these specific numbers do not have any significance. The different sputtering powers under the given base pressure and gas flow rate resulted in different oxygen concentrations in the Ti film. The target thickness of both Ti layers was achieved by adjusting the deposition time (90 and 13 min for 20 and 100 W, respectively), which was confirmed using scanning electron microscopy (SEM) (Hitachi, Model S-4800). Introducing different flows of oxygen during the sputtering resulted in the oxygen concentration in the film being too high, no matter how low the flow rate was in the present equipment. The crystalline structure of the Ti layer was examined by XRD (PANalytical, X'pert Pro) in θ–2θ mode. Subsequently, atomic layer deposited (ALD) TiO_2 films with the various thicknesses were grown on a Ti substrate at 250 °C as the dielectric of the SD. $Ti(OC_3H_7)_4$ and O_3 were used as the metal precursor and oxygen source, respectively. The intended ALD TiO_2 film thicknesses were 2.0, 4.2, 10.5, and 19.8 nm, respectively, which were attempted by controlling the number of ALD cycles. The growth rate of ALD TiO_2 film was ~0.035 nm/cycles. The film thickness was measured by an ellipsometer (Gaertner Scientific Corporation), using the TiO_2 films grown simultaneously on a Pt substrate. Details of the ALD process of TiO_2 film have been reported elsewhere.[15] Circular (6000 μm^2) and rectangular-shaped top electrodes (TEs) for electrical characteristics were fabricated by a conventional photolithography and lift-off process, using 50-nm-thick e-beam-evaporated Pt on the TiO_2 layer. The contact resistance (R_c) between the Ti layer and the Pt bottom electrode (BE) was evaluated by transmission line measurement (TLM). The Pt patterns for TLM were fabricated on Ti layer (150 nm)/SiO_2 (100 nm)/Si substrate. Current–voltage (I–V) characteristics of the SD were examined using an HP4145B semiconductor parameter analyzer (SPA) at room temperature in voltage sweep mode. The biases were applied to the TE, and the BE was electrically grounded during all of the measurements. The localized conduction paths of fabricated SD devices were investigated by CAFM (JEOL, JSPM-5200) measurement in both forward- and reverse-states with a positively and negatively biased Pt-coated cantilever, respectively. The chemical structures of the TiO_2 films in Ti substrates were examined by XPS equipped with Mg Kα as the X-ray source. The binding energies of the XPS spectra were calibrated by C–C bonding at the binding energy level of 285 eV in C 1s spectra. The chemical composition of the stacks was examined using the AES depth profiles.

RESULTS AND DISCUSSION

Figure 1a shows the XRD results of Ti layers that were deposited on Si substrates with sputtering powers of 20 and

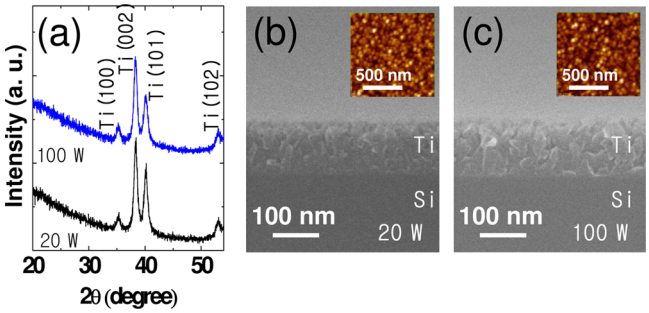

Figure 1. (a) XRD results of Ti layers with sputtering powers of 20 and 100 W deposited on Si substrates. Also shown are cross-sectional SEM images of Ti layers deposited on Si substrates with a sputtering power of (b) 20 W and (c) 100 W. The insets in panels (b) and (c) show the AFM topology of each Ti layer surface. (See ICDD Powder Diffraction File (PDF) Card No. 44-1294.)

100 W, respectively. Both Ti layers have a polycrystalline structure with similar preferred crystallographic orientations. The thicknesses of both Ti layers are almost the same (~150 nm), as shown in the SEM cross-sectional micrographs of Figures 1b and 1c. The surface roughness and the average grain size were measured via AFM, as shown in the insets of Figures 1b and 1c. The surface roughness of both Ti layers are almost similar: 3.16 and 3.08 nm for the sputtering power of 20 and 100 W, respectively. The average grain size of both Ti layers are also similar; ~ 58 and ~61 nm for the sputtering power of 20 and 100 W, respectively. Consequently, the differences in the physical structure of both Ti layers seems to be negligible, which would hardly affect the electrical characteristic of SD devices with the Ti layers.

Figures 2a and 2b show the AES depth profiles of Ti layer grown on the Pt substrate with sputtering powers of 20 and 100 W, respectively. Both Ti layers have the oxygen concentration throughout the film. It would be close to a highly oxygen-deficient TiO_{2-x} layer (x is ~1.25 and ~1.67 for the Ti layer grown with the sputtering power of 20 and 100 W, respectively) rather than pure Ti metal layer. Here, the AES concentration was calculated based on the assumption that the atomic concentration ratio of Ti:O = 1:2 for the ALD TiO_2 film, which was deposited on a Pt substrate (data not shown but is comparable to the surface composition of the films shown later in this paper in Figures 5d and 5h). Despite of considerable oxygen concentration in the Ti layer, the electrical pseudo-ohmic characteristic with the Pt BE can be maintained

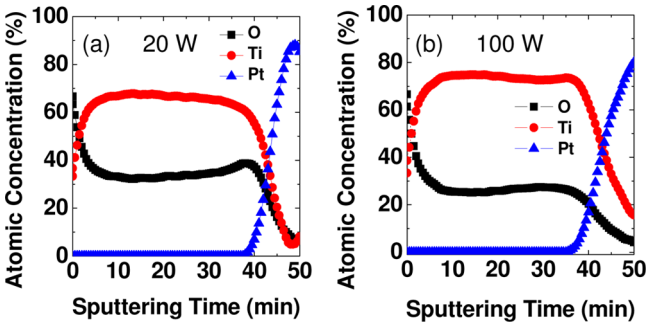

Figure 2. Auger electron spectroscopy (AES) depth profile results of Ti layers with sputtering powers of (a) 20 and (b) 100 W, respectively, on a Pt substrate.

due to the high conductivity of oxygen-containing Ti.[16] This suggests that the Ti layers can work as a substrate (electrode) in SDs, which will be demonstrated by the following experimental results.

The oxygen incorporated in the film during sputtering of the Ti layer originated from residual oxygen in the sputtering chamber. The oxygen concentration gradually decreased with growing Ti layers (decreasing etching time, except for the initial etching step of less than ~10 min) in the AES results, because the Ti metal getters the residual oxygen in the chamber during deposition. The higher oxygen concentration of the film surface is due to the natural oxidation of the film during the air exposure before the AES analysis. It was observed that the oxygen concentration in Ti layer is significantly decreased as the sputtering power is increased, because the high growth rate of the Ti layer decreased the chance for the oxygen to be incorporated into the film. The slow growth of Ti with the sputtering power of 20 W resulted in the obvious pileup of O atoms at the Ti/Pt interface, as shown in Figure 2a, while the faster growth of the same film with the sputtering power of 100 W did not induce such an obvious oxygen concentration gradient (Figure 2b). The oxygen was incorporated rather uniformly throughout the thickness in the latter case. The difference in oxygen concentration that induced the oxidation potential difference of Ti layer significantly affected the chemical composition of subsequently deposited ALD TiO_2 film, which are discussed with respect to the performances of SDs.

Figure 3 shows the variations of resistivity of Ti layers grown with sputtering powers of 20 W (black squares) and 100 W (blue circles), as a function of temperature. Here, the Ti layers were grown on thermal-oxidized SiO_2 (100 nm)/Si substrate for the sheet resistance (R_s) measurement using a four-point probe technique. The sheet resistance was measured every 5 s as the temperature was increased from 60 °C to 140 °C (1 °C/min). The resistivity was calculated using the measured sheet resistance and the thickness of Ti layer (~150 nm). Generally, the resistivity is much higher than that of pure Ti (42 $\mu\Omega$ cm at room temperature), because of the presence of a high concentration of oxygen. The resistivity increased gradually with increasing temperature for both Ti layers, which suggests that the both Ti layers have metallic electrical conduction characteristics, despite the considerable oxygen concentration. The resistivity of the Ti layer grown with a sputtering power of 20 W (563 $\mu\Omega$ cm at room temperature) was higher than that grown with a sputtering power of 100 W (155 $\mu\Omega$ cm at room temperature), because of the higher oxygen concentration. The resistance of Ti layer basically affects the performance of forward-current characteristic of SDs by changing the series resistance of the devices.[17] However, the difference in the resistivity would become negligible after the overlying TiO_2 layer deposition (the resistivity values of TiO_2(2 nm)/Ti stacked sample measured using a four-point probe technique were 1102 and 1060 $\mu\Omega$ cm at room temperature for the Ti layer grown with sputtering powers of 20 and 100 W, respectively), because of the increased oxygen concentration in the Ti layer by the overlying ALD process, which are discussed based on AES results.

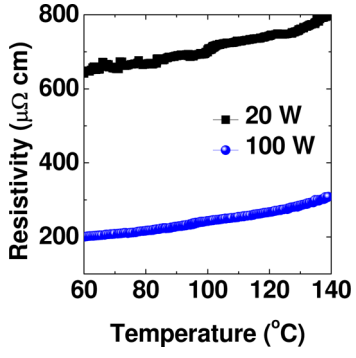

Figure 3. Resistivity measurement results with elevating temperature of Ti layers deposited on SiO_2 (100 nm)/Si substrate, with sputtering powers of 20 W (black squares) and 100 W (blue circles).

The R_c values between the Ti layer and the Pt BE also affects the forward-current characteristic of SDs, which was evaluated using TLM. The Pt patterns for TLM were fabricated on Ti layer (150 nm)/SiO_2 (100 nm)/Si substrate where six rectangular-shaped 50-nm-thick Pt electrodes with 200 μm width (w) were spaced with the distance (l) of 4, 9, 14, 19, and 24 μm, as shown in the inset of Figure 4. The linear electrical current−voltage (I−V) characteristics between every neighboring cell (not shown here) suggest the electrical Ohmic property of the Ti layer. The R_s and R_c values were evaluated using the slope and y-intercept of the plot of measured resistance values as a function of l/w in Figure 4, respectively. The resistivity values obtained here were consistent with those measured via the aforementioned four-point probe technique. (Values of 574 and 175 $\mu\Omega$ cm were obtained from the slopes of Figure 4 for

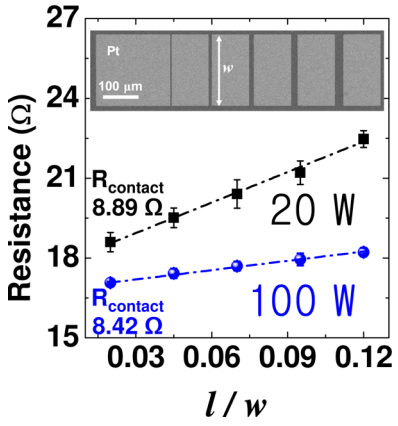

Figure 4. TLM results of Ti layers deposited on SiO_2 (100 nm)/Si substrate with sputtering powers of 20 W (black squares) and 100 W (blue circles).

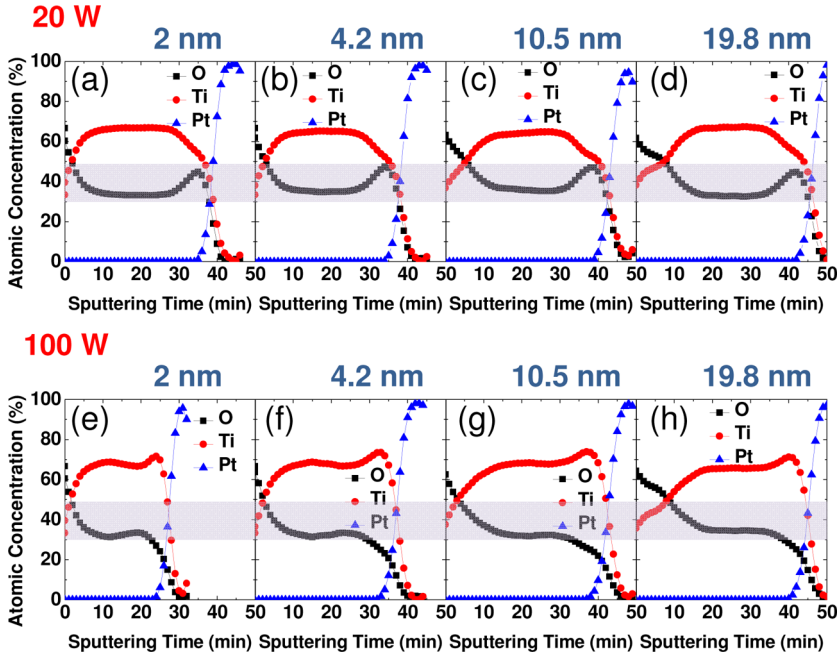

Figure 5. AES depth profiles of Ti substrates with sputtering powers of (a, b, c, d) 20 W and (e, f, g, h) 100 W after the various thicknesses (2, 4.2, 10.5, 19.8 nm) of ALD TiO_2 deposition on each Ti layer, respectively.

Ti layers with sputtering powers of 20 and 100 W, respectively, and values of 563 and 155 $\mu\Omega$ cm, respectively, were obtained for the same from the four-point measurements at room temperature.) R_c values for the Ti layer with sputtering powers of 20 and 100 W are 8.89 and 8.42 Ω, respectively. In comparison with the resistance values extracted from forward-state $I-V$ characteristic shown later in Figure 7 (306 and 277 Ω at 1 V for the case of a 19.8-nm-thick TiO_2 layer lying on a Ti layer with sputtering powers of 20 and 100 W, respectively), the R_c values are almost negligible. Consequently, the differences in the electrical properties of prepared Ti layer with the different sputtering powers have negligible influence on the electrical properties of fabricated SD.

However, the different oxygen concentration of the Ti layers crucially affects the stoichiometry of the ALD TiO_2 layer lying on it, which eventually determines the electronic Schottky barrier property of the ALD TiO_2 layer with a Pt TE. Figure 5 shows the AES depth profiles of ALD TiO_2 layer with the various thickenesses (2, 4.2, 10.5, 19.8 nm) on a Ti layer grown with sputtering powers of 20 and 100 W. The increased oxygen profiles near the surface region were observed clearly for all the cases due to ALD TiO_2 layers, while the thinnest TiO_2 case has little difference with the bare Ti layer, because of the presence of naturally oxidized layer on the Ti layer. The oxygen-rich layer became thicker with increasing thickness of ALD TiO_2 layer. Interestingly, the relative oxygen concentration in the bulk-region Ti layer grown with a sputtering power of 100 W increased largely after ALD of TiO_2 layer from ~25% to ~32%, while that in the Ti layer grown with a sputtering power of 20 W increased slightly from ~32% to ~33% after ALD of the TiO_2 layer. [See Figure 2.] This suggests that the O_3 gas supplied during the ALD process oxidized the underlying Ti layer, but under the given ALD condition of TiO_2 films, the maximum oxygen concentration of the nominally Ti layer does not exceed 33%. This enables the low resistance contact property to be maintained between this partly oxidized layer and the Pt BE. The initially higher oxygen concentration of the Ti layer grown with a sputtering power of 20 W retarded further oxidation, compared to the case with a sputtering power of 100 W during the ALD of TiO_2 film. It is interesting to note that the oxygen concentration in the bulk region of Ti layer reaches to a common value of 32%−33%, irrespective of the Ti sputtering power and the number of ALD cycles. Perhaps this concentration corresponds to a certain metastable state or full stuffing of grain boundaries with oxygen, but further research is certainly necessary in this regard.

It is one possibility that the O_3 consumption to oxidize the Ti layer may result in the oxygen-deficient ALD TiO_2 layer. Note that the ALD process for TiO_2 was optimized for the film growth on much less oxidative substrates, such as Si or Ru, and the strong oxidation potential of the Ti bottom layer may induce insufficiency of O_3 concentration to make the growing TiO_2 film stoichiometric. Because the Ti layer with 100 W has a higher oxidation potential than that of 20 W, this unfavorable situation could be further aggravated for this case. It is also possible that the oxygen in the ALD TiO_2 layer was consumed by the oxidation of the underlying Ti layer, even after the film was deposited via solid-state reaction. Therefore, severe oxidation of the Ti layer grown with a sputtering power of 100 W would induce greater oxygen deficiency of the overlying ALD TiO_2 layer. The stoichiometry of the ALD TiO_2 layer is crucial for achieving a sufficiently high Schottky barrier between TiO_2 and Pt TE in SDs, which is clearly shown in Figure 7 (below).

The variation in chemical binding status of the ALD TiO_2 layer with the various thicknesses, according to the sputtering powers of the underlying Ti layer growth, was examined in detail using XPS. Figures 6a and 6c show the Ti 2p core level XPS spectra for the ALD TiO_2 layer with various thicknesses on Ti layer grown with sputtering powers of 20 and 100 W, respectively. The binding energy of the Ti $2p_{3/2}$ peak for ALD TiO_2 films on Ti layer grown with a sputtering power of 100 W in Figure 6c is almost identical at a binding energy of ~458.9 eV, irrespective of the thickness of ALD TiO_2 film. Considering

dx.doi.org/10.1021/am301293v | ACS Appl. Mater. Interfaces 2012, 4, 5338−5345

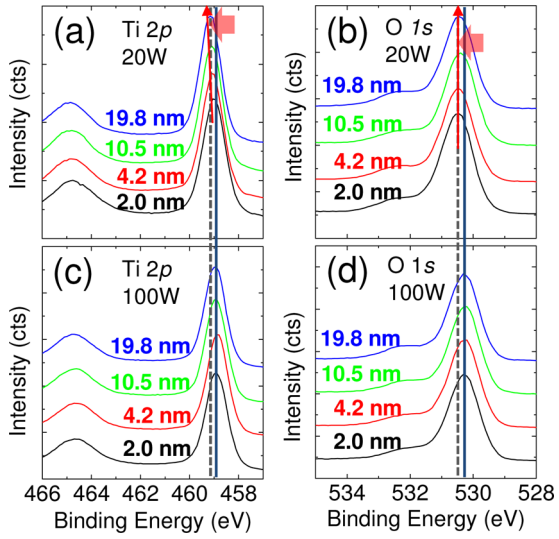

Figure 6. XPS analysis results according to each thickness of TiO_2 and sputtering deposition condition of Ti layer: (a) XP spectra of Ti 2*p*, relative to a surface TiO_2 layer deposited on a Ti layer with a sputtering deposition power of 20 W; (b) XP spectra of O 1*s*, relative to a surface TiO_2 layer deposited on a Ti layer with a sputtering deposition power of 20 W; (c) XP spectra of Ti 2*p*, relative to a surface TiO_2 layer deposited on a Ti layer with a sputtering deposition power of 100 W; and (d) XP spectra of O 1*s*, relative to a surface TiO_2 layer deposited on a Ti layer with a sputtering deposition power of 100 W. The dashed lines show the binding energy of Ti 2*p* (panels (a) and (c)) and O 1*s* (panels (b) and (d)) in stoichiometric TiO_2 thin films.[22]

that the probing depth of the XPS reaches to ~10 nm, the XPS signal for ALD TiO_2 films with thicknesses of 2.0 and 4.2 nm includes the chemical binding status information from the Ti layer. Therefore, the consistency in the binding energy of Ti $2p_{3/2}$ peak, even with increasing film thickness, suggests that the chemical binding status of the ALD TiO_2 film is similar to that of the Ti layer. This is because the Ti layer scavenged the oxygen from the ALD TiO_2 film, as mentioned above. The oxygen signal (Figure 6d) also showed the same trend. However, the binding energy of the Ti $2p_{3/2}$ peak for ALD TiO_2 films on the Ti layer grown with a sputtering power of 20 W increased as the film thickness increased. It shows that the ALD TiO_2 film became close to stoichiometry gradually as the thickness increased, because the higher oxygen concentration (lower oxidation potential) in the underlying Ti layer grown with the sputtering power of 20 W suppressed the oxygen consumption, compared to the other case. O 1*s* core level XPS spectra shown in Figures 6b and 6d also confirmed the improved stoichiometry of ALD TiO_2 film on Ti layer grown with the sputtering power of 20 W. The binding energies the O 1*s* main peak for ALD TiO_2 films on Ti layer grown with the sputtering power of 20 W (~530.5 eV) are higher than that in the case of 100 W (~530.3 eV). The shoulder peak at the bonding energy of ~532.5 eV corresponds to the carbonate phase in the TiO_2 film or surface contaminant, which is commonly observed in ex-situ XPS analysis of ALD metal-oxide film.[18]

Figures 7a and 7b show the *I*−*V* characteristics of SDs with the ALD TiO_2 films of various thicknesses on Ti substrates having Ti layers grown with sputtering powers of 20 and 100 W, respectively. Here, the electrode area was 6000 μm^2. First, the rectifying characteristics of both SDs are improved with increasing ALD TiO_2 thickness, regardless of the sputtering

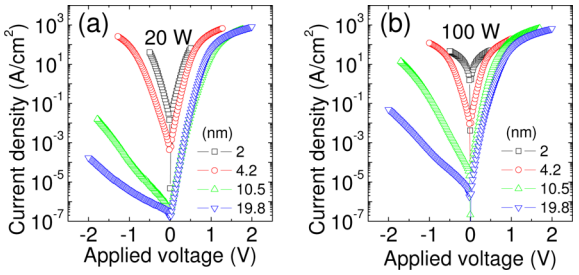

Figure 7. Electrical characteristic of SDs with various thicknesses of TiO_2 layers and Ti layers with the sputtering power of (a) 20 W and (b) 100 W.

power for Ti layer growth. Up to a TiO_2 thickness of ~4 nm, almost no rectification was observed and an Ohmic-like current flows for both cases, suggesting that such thin TiO_2 layers can barely form solid Schottky junctions with Pt, because of the severe oxygen loss by the reaction with underlying Ti. However, the samples show a certain rectification when the TiO_2 film becomes thicker than 10.5 nm. While the reverse current of the SDs was quite suppressed by increasing the ALD TiO_2 thickness, the decrease in the forward-state current density was not significant, compared to that of the reverse-state current. Since the main source of reverse current of the SDs is the electron injection from Pt TE through the ALD TiO_2 layer, the increased thickness of the ALD TiO_2 layer suppressed the current which might be related with tunneling and thermionic emission mechanisms.[19] In addition, the Ti layer consumed the oxygen from the ALD TiO_2 layer, which results in the high oxygen vacancy concentration near the interface with the Ti layer as well as non-negligible oxygen vacancy concentration near the interface between the TiO_2 and Pt TE. The very high leakage current, even under the negative bias when the TiO_2 thickness was less than ~4 nm, shown in Figure 7, suggests that the oxygen scavenging effect from TiO_2 by the Ti underlayer is significant throughout the entire thickness when the TiO_2 film was too thin. Therefore, an ALD TiO_2 layer with sufficient thickness is required to achieve a high electrical Schottky barrier with Pt TE and promising rectifying characteristics. The forward current is far less affected by the thickness of the ALD TiO_2 film, because the bulk resistance of the TiO_2 layer is generally much lower than that of Schottky contact under reverse bias.

The difference in the dissolved oxygen concentration in the Ti layer affects the oxygen vacancies generated in the ALD TiO_2 layer, as mentioned above. The higher oxygen concentration in the Ti layer grown with a sputtering power of 20 W suppressed the consumption of oxygen from the ALD TiO_2 layer, compared with the case of Ti layer grown with a sputtering power of 100 W. As the degradation of reverse leakage current in SD is dominantly governed by the defect (oxygen vacancy) density in the oxide layer in contact with the Schottky metal, the lesser loss of oxygen from the TiO_2 layer on the Ti layer grown with a sputtering power of 20 W results in the higher Schottky barrier at the Pt/TiO_2 interface. Therefore, the reverse current of SDs with the Ti layer grown with the sputtering power of 20 W is significantly lower than the other case as shown in Figure 7, which was observed obviously in the case with a thicker ALD TiO_2 layer (~10.5 and 19.8 nm). The better stoichiometry of the TiO_2 films on the Ti layer grown with a sputtering power of 20 W results in the higher series resistance for the forward bias, and, thus, the forward current

was generally lower, compared to the other case. However, the decrease in the reverse current was much larger, which eventually results in a much-higher rectification ratio of the sample with the Ti layer grown with a sputtering power of 20 W.

When the standard metal/semiconductor junction theory is applied, the depletion layer thickness (W) must be ~100 nm, assuming the donor concentration of 10^{18} cm^{-3} in TiO_2.[20] Actually, the donor concentration in the TiO_2 film showing good rectifying performance must be much lower than this value, suggesting that W must be even larger than this value. Therefore, the energy band structure of the $Pt/TiO_2/Ti$ structure must be effectively tilted (not curved) due to the work function mismatch between the Pt and Ti (or even the possible Fermi level pinning).[20] Pt/TiO_2 junction efficiently forms the Schottky-type blocking contact, while the Ti/TiO_x interface must be of a quasi-Ohmic nature, because of the lower work function of Ti and high defect density at that interface. When the Ti was grounded and Pt was biased to either positive or negative voltages, the forward or reverse current flows, which correspond to the diode $I-V$ curves shown in Figure 7. If the Pt/TiO_2 junction maintains its intact property, irrespective of the TiO_2 thickness and underlying Ti conditions, the reverse $I-V$ curves must be identical, which is obviously not the case in Figure 7. In principle, the Schottky barrier height (seen from the metal side) is independent of the dielectric thickness, while the diffusion potential seen from the dielectric side must be thickness-dependent when the total thickness is smaller than the depletion thickness.[20] The less TiO_2-thickness-dependent forward $I-V$ curves indicate that the quasi-Ohmic nature of the Ti/TiO_x interface is less influenced by the different process conditions. However, the highly TiO_2-thickness-dependent and Ti-condition-dependent reverse $I-V$ curves suggest that the Schottky barrier at the Pt/TiO_2 junction is highly dependent on the process conditions. This means that the Pt/TiO_2 junction is much more sensitive to the small change in the defect concentration in the TiO_2 layer.)

Figure 8 shows the summarized results of SDs performances (rectifying ratio, which was defined as the maximum ratio between the current measured at the same absolute value of positive and negative voltage for the two different oxygen concentrations in the Ti layer and the thickness of ALD TiO_2 layer. Because of the highly TiO_2-thickness-dependent $I-V$ characteristics, different voltages must be chosen for the different samples; here, 0.4 (0.2), 0.52 (0.32), 1.12 (0.7), and 1.26 (1.06) V, respectively, were taken as the read voltage for 2, 4.2, 10.5, and 19.8 nm, respectively, of TiO_2 layer lying on Ti layer with the sputtering power of 20 W (100 W). The excellent performance of SDs could be achieved by using the Ti layer with an initially higher oxygen concentration and a thicker ALD TiO_2 film. The maximum rectification ratio of ~10^7 was achieved from the sample with a 19.8-nm-thick TiO_2 layer deposited on a Ti layer with a sputtering power of 20 W.

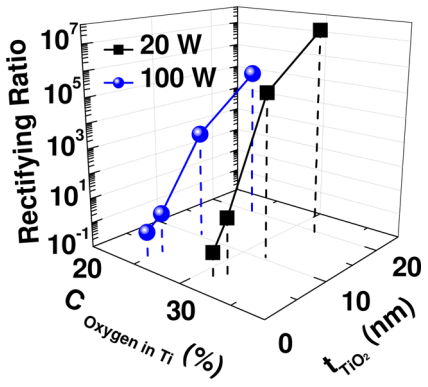

Figure 8. Summarized results on the rectifying ratio of the Schottky-type diode (SD), as a function of the thickness of ALD TiO_2 layer for different oxygen concentrations in the Ti layer.

A sufficiently high forward-current density of a SD is another key ingredient that the device must have, in addition to the high rectification ratio; otherwise, the SD adversely interferes with the RS of the memory element, which requires a very high current density. However, as is the case for the RS memory element using TiO_2 film, the current in SD can flow locally because of the inhomogeneity of the structure in atomic scale. Therefore, identifying the current flow pattern, even in SD, is crucial in estimating the ultimate current drivability of the SD. This can be done by CAFM.

CAFM measurement was carried out to examine the current conduction paths and their variations with the thickness of ALD TiO_2 layer and the sputtering power for Ti layer growth, which was summarized in Figure 9. Applied voltages of 3 V and −3 V to the Pt-coated cantilever were used for the forward- and reverse-state characteristics measurements, respectively, in a 1 μm × 1 μm scan area. The estimated values from CAFM should be compared relatively (not quantitatively) with the results obtained using SPA in Figure 7, because the Pt-coated cantilever with an approximate area of ~8×10^{-5} μm^2 has extremely higher contact resistance than the Pt TE of the stacked SDs used in measurement using SPA. While the bright spot denotes the high current conduction path in the forward-bias case, the dark spot denotes the high current conduction path in reverse-bias cases. In both cases with forward and reverse bias, local conduction paths for the current were observed, irrespective of the Ti layers. It is natural that the number of conduction paths decreased with increasing ALD TiO_2 thickness, because of the increased resistance. The inhomogeneous distribution of oxygen concentration near the interface between the ALD TiO_2 and the Ti layer induced a local conducting path, which remained as the conducting spots, even as the thickness of the ALD TiO_2 layer increased.[14] The forward current through the localized conduction paths is advantageous to provide sufficient current density to scaled RS cell,[14] where the forward current hardly depends on the scaled area of selection devices. In this point of view, the provided SD in this research fulfills the high rectifying ratio and high forward current density through the localized current conduction paths which are essential requirements for ReRAM application in CA-type devices. In ref 14, the authors reported that the forward-current density measured by the integration of the CAFM current was ~6.1×10^5 times smaller than that of the results from the pad-type measurement when the contact area was several square micrometers. The integrated forward-current density of the CAFM results shown in Figure 9 for the best case, i.e., 19.8-nm-thick TiO_2 on a 20 W Ti layer, was 0.7 A/cm^2, meaning that the same sample with the similar pad area, which was not fabricated in this experiment, because of the limited lithographic capability, would produce a current density of ~4.7×10^5 A/cm^2. This current density is sufficiently high for the operation of the RS memory cell in crossbar array architecture with at least 1 Mb block density.[21]

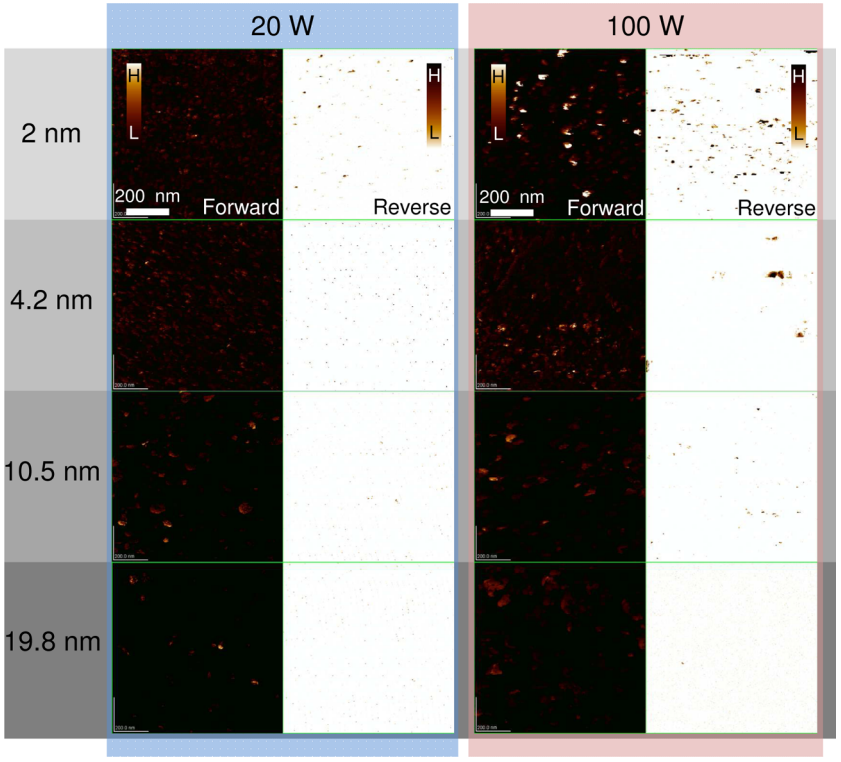

Figure 9. CAFM measurement results of individual SDs with variation of TiO_2 thickness and sputtering power of Ti layers.

In order to confirm the functionality of the optimized SD of this work, various stacked 1D1R CA array types (32 × 1, 2 × 2, 4 × 4, and 32 × 32) with line widths of 2, 4, 6, 8, and 10 μm were fabricated as an experimental demonstration. The unipolar memory cell was comprised of Pt/TiO_2/Pt, which is located below the optimized SD in the stacked 1D1R CA device structure, and the possible chemical reaction between the memory and SD was suppressed by the Ni layer interposed between them. Details of the fabrication process and electrical characterization results of the various CA devices are reported elsewhere.[23] Here, several representative data that show the suppression of sneak current in the CA with 4 × 4 configuration are presented. Figure 10a shows the plane-view SEM images of a 4 × 4 crossbar array with linewidths of 2 μm (upper figure) and 10 μm (lower figure), and Figure 10b shows the corresponding switching $I-V$ curves. It can be understood that the fluent resistance switching in the positive-bias region was achieved while the current flow in the negative-bias region was well-suppressed by the reverse action of the SD, suggesting the promising property of the CA as the resistance switching memory.

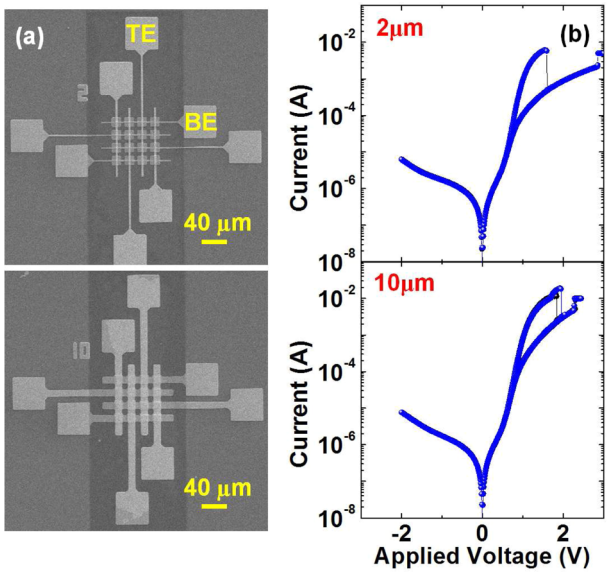

Figure 10. (a) Plane-view SEM images of a 4 × 4 crossbar array with linewidths of 2 μm (upper figure) and 10 μm (lower figure) having the stacked unipolar memory and Schottky-type diode, and (b) corresponding switching $I-V$ curves showing the fluent resistance switching in the positive-bias region while the current flow in the negative-bias region was well-suppressed by the reverse action of the Schottky-type diode.

CONCLUSIONS

In conclusion, two types of 150-nm-thick Ti substrates were prepared using different sputtering powers (20 and 100 W) during its deposition to control the oxygen concentration in the film. From the Auger electron spectroscopy (AES), sheet resistance measurement with elevating temperature and transmission line measurement (TLM) analysis, it was revealed that the Ti substrates with different deposition conditions have almost-identical physical structures but different dissolved oxygen concentrations. As the sputtering power increased during deposition, the dissolved oxygen concentration in the Ti layer, which can affect the stoichiometry of subsequently deposited TiO_2 layer, decreased. That is, to achieve the solid electrical Schottky contact between the ALD TiO_2 layer and the Pt top electrode (TE), a high oxygen concentration in the Ti layer, which does not disturb the pseudo-Ohmic contact characteristic with Pt bottom electrode (BE), and sufficient thickness of the TiO_2 layer should be needed. The AES and X-ray photoelectron spectroscopy (XPS) analysis of various

dx.doi.org/10.1021/am301293v | ACS Appl. Mater. Interfaces 2012, 4, 5338−5345

TiO_2/Ti/Pt stacked samples also demonstrated the importance of oxygen concentration of Ti layer and ALD TiO_2 thickness for excellent performance of Schottky-type diodes (SDs). When the Ti layer was deposited with a sputtering power of 20 W, which resulted in the initial oxygen concentration of ~32% and oxygen concentration of ~33% after the ALD TiO_2 with a thickness of ~20 nm, the Pt/TiO_2/Ti(O)/Pt SD produced a rectifying ratio of ~10^7 at the measurement voltage of 1.26 V. In addition, conductive atomic force microscopy (CAFM) measurements showed the existence of localized current conduction paths in the presented SDs, which are advantageous to provide a high forward-current density as well as a high rectifying ratio in highly scaled crossbar array (CA) devices. The indirectly estimated maximum current density from the CAFM was as high as 4.7×10^5 A/cm^2. The feasible memory operation of stacked 1D1R CA was also demonstrated.

AUTHOR INFORMATION

Corresponding Author

*E-mail: cheolsh@snu.ac.kr.

Author Contributions

The manuscript was written through contributions of all authors. All authors have given approval to the final version of the manuscript.

Notes

The authors declare no competing financial interest.

ACKNOWLEDGMENTS

This study was supported by the National Research Program for Nano Semiconductor Apparatus Development sponsored by the Korean Ministry of Knowledge and Economy, and the Convergent Research Center Program (No. 2012K001299) through the National Research Foundation of Korea funded by the Ministry of Education, Science, and Technology.

REFERENCES

(1) Waser, R.; Aono, M. *Nat. Mater.* **2007**, *6*, 833−840.

(2) Kim, K. M.; Jeong, D. S.; Hwang, C. S. *Nanotechnology* **2011**, *22*, 254002.

(3) Lee, M. J.; Park, Y.; Suh, D. S.; Lee, E. H.; Seo, S.; Kim, D. C.; Jung, R.; Kang, B. S.; Ahn, S. E.; Lee, C. B.; Seo, D. H.; Cha, Y. K.; Yoo, I. K.; Kim, J. S.; Park, B. H. *Adv. Mater.* **2007**, *19*, 3919−3923.

(4) Lee, M.-J.; Park, Y.; Kang, B.-S.; Ahn, S.-E.; Lee, C.; Kim, K.; Xianyu, W.; Stefanovich, G.; Lee, J.-H.; Chung, S.-J.; Kim, Y.-H.; Lee, C.-S.; Park, J.-B.; Yoo, I. K. In *Electron Devices Meeting, 2007 (IEDM 2007)*; IEEE International: New York, 2007; pp 771−774.

(5) Lee, M. J.; Kim, S. I.; Lee, C. B.; Yin, H.; Ahn, S. E.; Kang, B. S.; Kim, K. H.; Park, J. C.; Kim, C. J.; Kim, S. W.; Stefanovich, G.; Lee, J. H.; Chung, S. J.; Kim, Y. H.; Park, Y. S. *Adv. Funct. Mater.* **2009**, *19*, 1587−1593.

(6) Kang, B. S.; Ahn, S. E.; Lee, M. J.; Stefanovich, G.; Kim, K. H.; Xianyu, W. X.; Lee, C. B.; Park, Y. S.; Beak, I. G.; Park, B. H. *Adv. Mater.* **2008**, *20*, 3066−3069.

(7) Park, W. Y.; Kim, G. H.; Seok, J. Y.; Kim, K. M.; Song, S. J.; Lee, M. H.; Hwang, C. S. *Nanotechnology* **2010**, *21*, 195201.

(8) Shin, Y. C.; Song, J. W.; Kim, K. M.; Choi, B. J.; Choi, S.; Lee, H. J.; Kim, G. H.; Eom, T. Y.; Hwang, C. S. *Appl. Phys. Lett.* **2008**, *92*, 162904.

(9) Huby, N.; Tallarida, G.; Kutrzeba, M.; Ferrari, S.; Guziewicz, E.; Wachnicki, Ł.; Godlewski, M. *Microelectron. Eng.* **2008**, *85*, 2442−2444.

(10) Chang, S. H.; Lee, S. B.; Jeon, D. Y.; Park, S. J.; Kim, G. T.; Yang, S. M.; Chae, S. C.; Yoo, H. K.; Kang, B. S.; Lee, M. J.; Noh, T. W. *Adv. Mater.* **2011**, *23*, 4063−4067.

(11) Lee, J. H.; Kim, G. H.; Ahn, Y. B.; Park, J. W.; Ryu, S. W.; Hwang, C. S.; Kim, H. J. *Appl. Phys. Lett.* **2012**, *100*, 123505.

(12) Linn, E.; Rosezin, R.; Kügeler, C.; Waser, R. *Nat. Mater.* **2010**, *9*, 403−406.

(13) Zuo, Q.; Long, S.; Liu, Q.; Zhang, S.; Wang, Q.; Li, Y.; Wang, Y.; Liu, M. *J. Appl. Phys.* **2009**, *106*, 073724.

(14) Kim, G. H.; Lee, J. H.; Han, J. H.; Song, S. J.; Seok, J. Y.; Yoon, J. H.; Yoon, K. J.; Lee, M. H.; Park, T. J.; Hwang, C. S. *Appl. Phys. Lett.* **2012**, *100*, 213508.

(15) Choi, G. J.; Kim, S. K.; Lee, S. Y.; Park, W. Y.; Seo, M. H.; Choi, B. J.; Hwang, C. S. *J. Electrochem. Soc.* **2009**, *156*, G71−G77.

(16) Kwon, D. H.; Kim, K. M.; Jang, J. H.; Jeon, J. M.; Lee, M. H.; Kim, G. H.; Li, X. S.; Park, G. S.; Lee, B. R.; Han, S. W.; Kim, M. Y.; Hwang, C. S. *Nat. Nanotechnol.* **2010**, *5*, 148−153.

(17) Cheung, S. K.; Cheung, N. W. *Appl. Phys. Lett.* **1986**, *86*, 280085.

(18) B. Vincent Crist *Handbook of Monochromatic XPS Spectra: The Elements and Native Oxides*; Wiley: New York, 2000.

(19) P. Hesto In *Instabilities in Silicon Devices*; Barbottin, G., Vapaille, A., Eds.; Elsevier Science Publishers B.V.: Amsterdam, 1986; Vol. *1*, pp 295−297.

(20) P. Hesto In *Instabilities in Silicon Devices*; Barbottin, G., Vapaille, A., Eds.; Elsevier Science Publishers B.V.: Amsterdam, 1986; Vol. *1*, p 275.

(21) Kim, G. H.; Kim, K. M.; Seok, J. Y.; Lee, H. J.; Cho, D. Y.; Han, J. H.; Hwang, C. S. *Nanotechnology* **2010**, *21*, 385202.

(22) Stefanov, P.; Shipochka, M.; Stefchev, P.; Raicheva, Z.; Lazarova, V.; Spassov, L. *J. Phys.: Conf. Ser.* **2008**, *100*, 012039.

(23) Kim, G. H.; Lee, J. H.; Ahn, Y.; Jeon, W.; Song, S. J.; Seok, J. Y.; Yoon, J. H.; Yoon, K. J.; Park, T. J.; Hwang, C. S. *Adv. Funct. Mater.*, **2012**, in press (DOI: 10.1002/adfm.201202170).